Starburst Nuclei and Cosmic-Rays Transport Mechanisms: future Opportunities for Neutrino Astronomy and Beyond Standard Model Studies

Antonio Ambrosone[1,2,*], *Marco* Chianese[1,2], *Damiano F.G.* Fiorillo[5], *Antonio* Marinelli[1,2,4], and *Gennaro* Miele[1,2,3]

[1]Dipartimento di Fisica "Ettore Pancini", Università degli studi di Napoli "Federico II", Complesso Univ. Monte S. Angelo, I-80126 Napoli, Italy
[2]INFN - Sezione di Napoli, Complesso Univ. Monte S. Angelo, I-80126 Napoli, Italy
[3]Scuola Superiore Meridionale, Università degli studi di Napoli "Federico II", Largo San Marcellino 10, 80138 Napoli, Italy
[4]INAF-Osservatorio Astronomico di Capodimonte, Salita Moiariello 16, I-80131 Naples, Italy
[5]Niels Bohr International Academy, Niels Bohr Institute, University of Copenhagen, Copenhagen, Denmark

Abstract. Experimental observations have demonstrated a strong correlation between star-forming processes and gamma-ray luminosities, giving strong hints about the nature of the Cosmic-Rays (CRs) transport mechanisms inside Starburst Nuclei. In this contribution, we discuss the imprints on nearby Starburst galaxies (SBGs) gamma-ray spectra left by different CR transport models, quantifying the potentiality of future telescopes to distinguish between them. We also investigate the possibility of constraining the properties of light Dark Matter (DM) particles exploiting the peculiar nature of CR transport inside SBNs. We show that the property of scattering between high-energy CRs and DM particles leads to observable features, thereby posing stringent constraints on the DM parameter space.

1 Introduction

Starforming and Starburst Galaxies (SFGs and SBGs) are peculiar astrophysical sources which are expected to inject and accelerate high-energy CRs in their cores (see [1–6] and Refs. therein). Indeed, some nearby SBGs have been discovered as a GeV gamma-ray emitters [7]. Furthermore, M82 and NGC 253 have also been detected in the TeV domain by respectively VERITAS [9] and HESS detectors [10]. The Auger collaboration has also found a correlation of about $\sim 4\,\sigma$ with some of these sources and ultra high-energy cosmic-rays [11]. All of these demonstrate, to some extent, that SBGs produce high-energy CRs (at least up to $\sim$ 1 PeV energy) and are able to confine them for long enough to produce secondary particles such gamma-rays and probably neutrinos. Indeed, high-energy cosmic rays are expected to be accelerated by supernovae explosions (SNe) and they should collide with interstellar medium particles producing secondary particles through inelastic p-p collisions. The spectra of secondary particles strictly depend on the parent high-energy protons distribution in starburst nuclei (SBNi)[5]. As a result, the cosmic-ray transport mechanisms are expected to leave indelible signatures on the gamma-ray and neutrino spectra which are observables. Therefore, we can use these as indirect tools to study the properties of the transport conditions inside SBGs, which are still under debate [5, 6, 16]. In fact, while electrons are predominatly confined inside the starburst nuclei, the high-energy protons are only partially confined and it is still unclear which is the main escape phenomenon out of SBNi: advection or diffusion [5] (see also [16]). Furthermore, it is still not completely clear which is the source of the diffusions mechanisms. For instance, Refs. [1–4] indicate external turbulence as diffusion mechanism, while Refs. [13–15] have proposed diffusion driven by self-induce interactions with Alfen waves generated though streaming instability. In this proceeding, we analyze the imprints left by different cosmic-ray transport mechanisms inside SBGs on gamma-ray observations (see [5] for more details). In particular, we demonstrate how the next-generation CTA telescope and SWGO are going to discriminate between different cosmic ray transport mechamisms. Furthermore, our findings suggest that advective phemonena seem to be preferable as escape mechanism until $E \sim 10 - 100$ TeV for protons [5]. We also exploit the nature of our results to perform a beyond standard model study [6]. In fact, a potential interaction between a dark-matter particle χ and protons would modify the gamma-ray spectra leading to a depletion of photons, which is not currently observed. Therefore, this leads to strict bounds on $\sigma_{\chi,p} \sim 10^{-32}\,\mathrm{cm}^2$ for $m_\chi \leq 10^{-6}$ GeV [6]. The proceeding is structured as follows: in Sec. 2, we discuss the CR transport models considered in our analysis and how we evaluated the secondary particle production rates. In Sec. 3, we discuss the different gamma-ray phenomenology arising from the corrisponding CR transport models and in Sec. 4 we discuss possible incoming constraints from neutrino telescopes. On the other hand, In Sec. 5, we discuss the implications of scattering between sub GeV DM particles and cosmic rays inside SBNi. Fi-

*e-mail: antonio.ambrosone@unina.it

nally, in Sec. 6 we discuss all the results and derive our conclusions.

2 Cosmic-ray Mechanims Models and Secondary Particles

Many authors have described the cosmic-ray transport mechanisms inside SBGs [1, 2, 13, 16–18, 22](see also [4, 5] and Refs therein for more details). In particular, we work in a steady-state assumptions, leading to a balance between the high-energy cosmic rays injected by SNe and all the mechanisms such as p-p interaction, advection and diffusion occuring inside Starburst Nuclei (SBNi) [5]. Therefore, the proton distribution $f(p)$ inside the nuclei can be written as [5]

$$f(p) = Q(p) \cdot \tau_{pp} \cdot F_{\rm cal}(p) \tag{1}$$

where $Q(p) \propto (p/mp)^{-\alpha} \times e^{-p/p_{max}}$ is the injected amount of high-energy cosmic rays from SNe with $p_{max} \sim 1-10\,$PeV [1–6]. τ_{pp} is the proton-proton interaction timescale:

$$\tau_{pp} = \frac{1}{k \cdot n_{\rm ISM} \cdot \sigma_{pp} \cdot c} \tag{2}$$

where $k = 0.5$ is the inelasticity of the process. c is the light velocity. $n_{\rm ISM}$ is the interstellar medium density. σ_{pp} is the inelastic cross section [20]. $F_{\rm cal}(p)$ is the calorimetric fraction, namely the fraction of high-energy protons which effectively lose energy inside the nucleus producing gamma-rays and neutrinos rather than escape via advection or diffusion. $F_{\rm cal}(p)$ theoretically depends on the geometrical assumptions of the system (e.g. spherical, cilindrical or even toroidal). This is because under a different geometries, protons can escape differently from the nucleus. Secondly, different assumptions on the escape mechanisms can affect the energy-dependency of $F_{\rm cal}$. In this proceeding, along with Ref. [5], we quantify the differences between the CR model developed by Ref. [1, 2] which was also used by Ref. [3–6] and the model put forward by [13] which was also used by Ref. [14, 15]. The former, which we call model A (see also [5] for more details), assumes that the nucleus is spherical and the diffusion is described by a Kolmogorov-like scenario in a regime of strong turbulence with an external magnetic field B. Given R as the dimension of the nucleus, the diffusion timescale $\tau_{\rm diff} = R^2/D$ where D is the diffusion coefficient (see [1] for more details). The model takes also into account the advection phenomen which consist in cosmirays driven by the motion of the interstellar medium. Indeed, given v the wind velocity, the advection timescale $\tau_{\rm adv} = R/v$. In this model, the escape mechanims is given by the competition between $\tau_{\rm adv}$ and $\tau_{\rm diff}$. In fact, the escape timescale is $(\tau_{\rm adv}^{-1} + \tau_{\rm diff}^{-1})^{-1}$ [5]. For this model the calorimetric fraction can be express as [5]:

$$F_{\rm cal} = \frac{\tau_{esc}/\tau_{pp}}{\tau_{esc}/\tau_{pp} + 1} \tag{3}$$

where $\tau_{\rm eff} = \tau_{esc}/\tau_{pp}$. In this model, $\tau_{\rm diff} > \tau_{\rm adv}$, hence the escape timescale is driven by the winds. The latter, namely model B, on the other hand, assumes a cilindrical geometry and, consequently, the calorimetric fraction is given by [5, 13–15]:

$$F_{\rm cal} = 1 - \left[{}_0F_1\left(\frac{1}{5}, \frac{16}{25}\tau_{\rm eff}\right) + \frac{3\tau_{\rm eff}}{4M_A^3}\, {}_0F_1\left(\frac{9}{5}, \frac{16}{25}\tau_{\rm eff}\right)\right]^{-1} \tag{4}$$

where $M_A \simeq 2$ is the mach number and ${}_0F_1$ is the generalized hypergeometric function [13–15]. The cosmic ray transport description, in this model, is different since neglects advection phenomena arguing that they could only affect the ionised gas and it is still not clear whether they could also affect the cold interstellar medium gas or not. Furthermore, it considers diffusion driven by the self-turbulence by the alven waves generated by CRs themselves. In this framework the diffusion coefficient is proportional to the streaming velocity of cosmic rays [5, 13–15]:

$$D \propto V_s = {\rm Min}\Big[{\rm c}, {\rm V_{al}}(1 + 2.3 \cdot 10^{-3} \cdot \Big(\frac{\rm E}{\rm m_p}\Big)^{\alpha-3} \times \times \Big(\frac{n_{\rm ISM}}{10^3}\Big)^{3/2} \Big(\frac{\chi}{10^{-4}}\Big) \Big(\frac{\sigma_g}{10\sqrt{2}\,{\rm Kms^{-1}}}\Big)\Big] \tag{5}$$

where σ_g is the dispersion velocity, χ is the ionisation fraction. E and m_p are respectively proton energy and mass. τ_{diff} in model B is defined as h^2/D where h is the height of the galatic disk. One of the differences between model A and model B is that in the former the calorimetric fraction is practically energy independent up to $\sim 1\,$PeV, while for the latter it has a strong trend with energy. Indeed, above $\sim 100\,$GeV $-$ 1 TeV SBGs stop being calorimetric leading to a suppresion to the consequent gamma-ray and neutrino production.

In both models, the main contribution to the gamma-ray and neutrino production is given by hadronic production, which we evaluate using the delta-function approximation following [20]. We also take into account bremsstrahlung and Inverse Compton contributons following [4, 5]. We finally emphasize that we neglect gamma-ray and neutrino production due to photo hadronic ($p\,\gamma$) collisions due to the fact that the energy threshold for such process requires CR energy to be greater than $\simeq 150\,$PeV which is a scenario which we do not consider. Furthermore, Refs. [18, 19] have demonstrated that their contribution is completely negligible with respect to the p-p collision component.

3 Gamma-ray Phenomenology

In order to analyze the different phenomenology arising from model A and model B, we fit gamma-ray data of known SFGs and SBGs (see [5] for more details). The gamma-ray data analized are the *Fermi*-LAT data from [7, 21]. For M82 and NGC 253, we also take into account VERITAS [9] and HESS [10] data. We consider as free parameters the star formation rate $\dot{M}$ of the source as well as the spectral index α (see [5] for details about the values of the other structural parameters used). We stress that we impose the star formation rate of the source to be

consistent with the one inferred by experimental data [16] within a factor 3 [5].

Fig. 1 shows the comparison between the best-fit obtained from model A and B and its current gamma-ray data [7, 9].

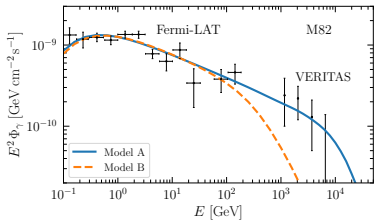

Figure 1. Comparison between the gamma-ray best fit from model A and model B for M82 and its gamma-ray data [7, 9]. Figure taken from Ref. [5].

Interestingly, model A seems to slighly fit better the gamma-ray data. Indeed, model B seems to be disfavoured at 2σ level [5]. This seems to slightly point towards the conclusion that phenomenlogically advection phenomena might be important for describing the escape mechanisms inside starburst nuclei (SBNi). Indeed, the fact that gamma-ray data are compatible with a simple power-law spectrum might be indicative of CRs dominated by energy-independent timescales [22]. Future experimental campaigns will be fundamental in order to get more and more precise data. In particular, the CTA telescope [26] will provide measurements increasing the statistical power in order to distinguish between model A and model B [5] (take a look also at Refs. [27, 28] the potentiality of the ASTRI-mini array to fully understand the potentiality of Imagine Atmosphere Cherenkov Telescopes (IACTs). We end this section by saying that also other experiments could be able to constrain phenomenological properties of SBNi such as SWGO [29].

4 (Potential) Future Neutrino Constraints

Different CR transport descriptions lead to different neutrino spectra expectations as well. In this section, focusing on model A, we show the prospects for future constrains from current and upcoming high-energy neutrino telescopes (following Ref. [4]). Fig. 2 shows the comparison between the expected 1 TeV neutrino normalizations from nearby SFGs and SBGs with the point-like IceCube sensitivity [23] and the expected sensitivity of the KM3NeT/ARCA [24] detector and ICeCube gen 2.

Interestingly, KM3NeT/ARCA [25] could constrain the hadronic emissions of the cores of Small Magellanic Cloud (SMC) and Circinus Galaxy in 6 years of data taking. It is important to say that the sensitivities refer to E^{-2} spectra while the neutrino expectations of the sources might be slightly softer (see [4] for more details). Nonetheless, the emission of the core of SMC could be constrained in 6 years of data taking. The next decade will be fundamental for constraining the property of SFGs

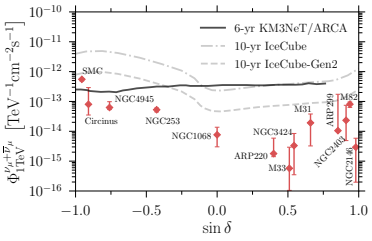

Figure 2. Comparison between the 1 TeV neutrino normalizations according to model A (see [4] for more details) and the IceCube, KM3NeT and IceCube Gen 2 sensitivities for E^{-2} point-like sources. Figure taken from Ref. [4].

and SBGs. Indeed, a potential neutrino emission measurement from these sources not only would demonstrate that star formation processes can emit neutrinos but also they will allow incredible step forward for understanding the CR transport inside these sources.

5 DM-p Interactions

In the previous sections, we have analized the CR transport mechanisms inside SBGs. It seems that current data slightly favour model A. In this section, we exploit this fact in order to search for new physics. In particular, astrophysical and cosmological observations show that galaxies have a halo of dark matter (DM) [34–41]. Therefore, a potential interaction between a DM particle (χ) and protons could modify the CR transport inside the SBGs leading to a suppression of the secondary particles fluxes. For instance, a further a loss timescale $\tau_{\rm loss}$ modifies $\tau_{\rm esc}$ in Eq. 3 leading to a different $F_{\rm cal}$. The new timescale is

$$\tau^{\rm el}_{\chi p} = \left[\frac{-1}{E}\left(\frac{dE}{dt}\right)_{\chi p}\right]^{-1} \tag{6}$$

which represent the elastic timescale between χ and protons. dE/dt is the time rate with which CR exchange energy with dark matter particles. It strictly depends on the DM density ρ_χ as well as on the elastic cross section $\sigma_{\rm el}$ [6]:

$$\left(\frac{dE}{dt}\right)_{\chi p} = \frac{\rho_\chi}{m_\chi}\int_0^{T^{\rm max}} dT_\chi T_\chi \frac{d\sigma_{\rm el}}{dT_{\rm el}} \tag{7}$$

where $T^{\rm max}$ is the maximal kinetic energy allowed by DM particles in a collision with a proton with energy E. The expression of $T^{\rm max}$ can be found in Ref. [6] and in Refs. therein. For this contribution (see Ref. [6] for more details), we consider the DM particle to be a fermion interacting with protons through a high massive mediator. In this context, the differential elastic cross section is [6, 30]:

$$\frac{d\sigma_{\rm el}}{dT_\chi} = \begin{cases} \frac{\sigma_{\chi p}}{T^{\rm max}}\frac{F^2(q^2)}{16\mu^2_{\chi p}s}(q^2+4m_p^2)(q^2+4m_\chi^2) & \text{if } T_\chi < T^{\rm max} \\ 0 & \text{if } T_\chi > T^{\rm max} \end{cases} \tag{8}$$

where $\sigma_{\chi p}$ is the DM-p at zero CM momentum [6]. $\mu_{\chi p}$ is reduced mass between χ and protons. $s = m_\chi^2 + m_p^2 + 2Em_\chi$

is center of mass energy. $F(q) = (\frac{1}{1+q^2/\Lambda^2})^2$ (with $q^2 = 2m_\chi T_\chi$) is the proton form factor. This factor practically implies that at high-energy the elastic collision becomes unlikely with respect to the inelastic one. Indeed, for energies $E > m_p^2/(2m_\chi)$ the proton start being broken, producing additional gamma-rays through pion decay. We parametrize the inelastic collisons between χ and protons, using a simple semy-analytical approximation (similarly to [31–33]) assuming the $\sigma_{\mathrm{inel}\,\chi\mathrm{p}}$ scales as the νp (neutrino nucleon) cross section and rescaling it to match the elastic χp cross section [6]. This allows us to define the inelastic cross section as a function of $\sigma_{\chi p}$ defined in Eq. 8 (see [6] for more details). The inelastic collisions timescales can be defined analogously to the proton proton collisions as $\tau_{\mathrm{inel}} = \left(k\sigma_{\mathrm{inel}} \cdot c\,\rho_\chi/m_\chi\right)^{-1}$, where k is the inelasticity of the collision and ρ_χ is the DM energy density. We consider $k = 0.5$ analogously to p-p collisions [6].

5.1 Dark Matter Density inside Starburst Nuclei

Each galaxy is expected to be embedded in a Dark Matter halo [34–41]. The *correct* DM profile is still uncertain because of the uncertainty in the DM distribution in the core of the galaxies [42] (see also [6] and Refs. therein for further details). One of the benchmarks which can be used are the NFW profile [43]:

$$\rho_{DM}(r) = \rho_s \frac{1}{r/r_s(1 + r/r_s)^2} \tag{9}$$

Another benchmark DM density profile is the Burkert profile [44]:

$$\rho_{DM}(r) = \frac{\rho_0 r_s^3}{(r + r_s)(r^2 + r_s^2)} \tag{10}$$

where r represents the distance between the DM halo. We consider it to be also coincident with the position of the Starbust Nucleus of the SBG considered. In order to parametrize ρ_s, r_s and ρ_0 for the two cases, we follow Refs. [37–39, 41]. In particular, we do it by means of c_{200} and M_{200}. $c_{200} = r_{200}/r_s$, where r_{200} is the radius corresponding to M_{200} where the mean density is 200 times the critical density of the Universe [6]. These two parameters are not measured, but they are constrained by cosmological simulations to be $7 \leq c_{200} \leq 12$ and $10^{10} \leq M_{200}/M_\odot \leq 10^{12}$ [37–39, 41]. Fig. 3 shows the DM density distribution for both benchmark cases. In particular, the blue band corresponds to the NFW profile and the orange one corresponds to the Burkert one. The main difference between the NFW and Burkert profile resides in the fact that the former is divergent for $r \to 0$. The figure also shows the value corresponding to $r = R_{\mathrm{SBN}} = 200\,\mathrm{pc}$ which corresponds to a benchmark value of a prototypical SBN (see also [1, 2, 4, 5]).

5.2 Signatures on Gamma-ray Spectra: M82 Example

In this section, we analyse which are phenomenological signatures of DM-p interactions. Fig. 4 shows the case of M82.

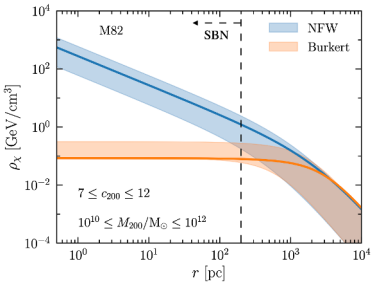

Figure 3. DM energy density as a function of r. The Blue band corresponds to the NFW profile, while the orange one corresponds to the Burkert profile. The vertical line correspond to the dimension R of a typical starburst nucleus $R = 200\,\mathrm{pc}$.

In particular, on the left panel, we show the comparison between the standard timescales (losses, advection and diffusion) as black lines with the elastic and the inelastic DM-p interaction timescales for three different values of $(m_\chi, \sigma_{\chi p})$. $\tau_{el}^{\chi p}$, for $E_p \leq E_{\mathrm{min}} = m_p^2/2m_\chi$, scales as T^{-3}, where T is the proton kinetic energy. By constrast, for $E > E_{\mathrm{min}}$, $\tau_{el}^{\chi p} \sim T^3 \times \mathrm{Log(T)}$ (see [6] for more details). As a result, at high energies ($E > E_{\mathrm{min}}$), the elastic collisions become unlikely leading to a strongly energy- increasing timescale. The right panel of Fig. 4 shows the corresponding the gamma-ray spectrum predicted. The black line corresponds to the standard scenario (model A), while the coloured lines correspond to the gamma-rays with DM-p interactions. The elastic collisions clearly reduce the spectrum leading to a dip in the gamma-ray spectrum. This is due to the fact that protons interacting with χ reduce their energy without producing gamma-rays. In practice this strongly reduces F_{cal}. For $E_\gamma \gtrapprox 0.1 E_{\mathrm{min}}$ (the ~ 0.1 factor is due to the fact that gamma-rays produced through pion decays carry about $1/10$ of the energy of the parent high-energy proton), the gamma-rays get replenished by the photons produced by inelastic DM-p collisions. Indeed, in this regime, SBGs start being calorimetric again leading to a copious gamma-rays production. It is important to highlight that for energies greater than E_{min}, $F_{\mathrm{cal}} \to 100\%$. On the contrary, in the standard scenario $F_{\mathrm{cal}} \sim 40$–50% given the competition between advection and p-p timescales. All of this leads to a higher normalization after the dip.

5.3 Phenomenological Constraints On $\sigma_{\chi p}$

The signature of DM-p interaction might significantly modify the gamma-ray spectrum of the SBG. Therefore, current data can be used to put strict constraints on $\sigma_{\chi p}$. For this purpose, following Ref. [6], we analyze the gamma-ray data of two nearby SBNi: M82 and NGC 253. In particular we analyze 10-year data of Fermi-LAT data [7] as well as VERITAS [9] and HESS [10] data respectively for M82 and NGC 253. We perform the statistical analysis following Refs. [4–6]; indeed, the likelihood is defined by $\mathcal{L} = e^{-\frac{1}{2}\chi^2}$, where $\chi^2 = \sum_i (SED_i - E_i^2 \phi(E_i, m_\chi, \sigma_{\chi p}|\theta))^2/\sigma_i^2)$, where i runs over all the measurments [4–6] and θ represents all the astrophysical parameters treated as nuisance parameters (see

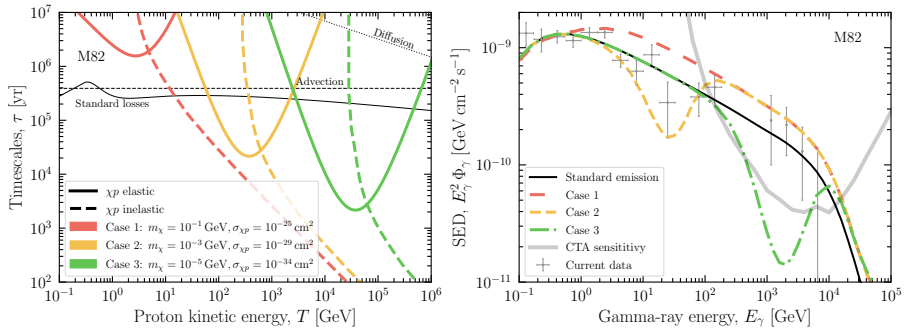

Figure 4. Left Panel The comparison between the *standard* timescales (losses, advection and diffusion) in black lines and three different cases regarding m_χ and $\sigma_{\chi p}$. Please be careful that in this figure the losses timescales are divided by $\alpha - 3$ [6]. **Right Panel** The corresponding theoretical expected gamma-ray fluxes for the source compared with the experimental Fermi-LAT and VERITAS data [7, 9]. Image taken from Ref. [6].

[6]). The bounds on $\sigma_{\chi p}$ by means of the test statistic: $\Delta\chi^2 = \chi^2(m_\chi, \sigma_{\chi p}) - \chi^2(m_\chi, 0)$ [6], where the chi squared is marginalised over the astrophysical parameters. The bounds are set with $\Delta\chi^2 = 23.6$, namely at 5σ level [6].

Fig. 5 shows the bounds imposed on $\sigma_{\chi p}$, on the left regarding M82, and on the right NGC 253. The blue band corresponds to the NFW profile and the orange band corresponds to the Burkert one. Indeed, the band mirrors the uncertainty on the cosmological parameters c_{200} and M_{200} of the DM halo. The shape of the bounds do not depend on the DM profile since the gamma-ray spectrum is dependent on the mean density in the SBN $\Phi_\gamma \propto \int \rho_\chi^{-1}(r)/VdV$ [6]. Indeed, the blue and the orange bands scale exaclty with the difference of the average DM density inside SBN. The results of the two sources slightly different because of the difference between the two datasets. For instance, at high energies NGC 253 has slighlty more and more precise data than M82. For $m_\chi \lessapprox 1$ KeV the bounds flatten because the $E_{\rm min} > 100$ TeV, corresponding to a dip in the gamma-ray spectrum at energies $E_\gamma > 10$ TeV which cannot be probed for these two extragalactic sources due to EBL absorption (see for instance [45]). The higher m_χ, the bounds weaken because of the proton form factor which make the elastic collision unlikely.

6 Discussion and Conclusions

In this contribution, we have showed several updates about the CR transport description inside SBNi. In particular, we have studied the gamma-ray and neutrino phenomenology of different CR transport description. Indeed, following Ref. [5], we have studied two different CR models: model A [1], in which the main escape CR phenomenon is advection, leading to a energy-independent calorimetric fraction. Model B [13], on the contrary, neglecting advection phenomena and considering diffusion caused by self-turbulence, leads to a energy-depedent calorimetric fraction above ~ 100 GeV, which makes SBNi totally non calorimetric. We have demonstrated that current gamma-ray seem prefering model A, pointing to a simple power-law spectrum. However, given the current astrophysical uncertainty, it is not possible to statistically distinguish between the models at more than $1 - 2\,\sigma$ [5]. Future experiments such as CTA [26], SWGO [29] and ASTRI mini array [27, 28] will be able to provide us with more pieces of information regarding these sources, solving the mystery of their CR transport mechanisms. We have also used model A in order to search for new physics. Indeed, a new interaction between a DM particle and protons strongly modifies the proton distribution inside the nucleus. Indeed, this would create a dip in the gamma-ray spectrum, namely modyfing the standard power-law spectrum. Since in the experimental data, there is no dip, we set strong constrains on the cross section $\sigma_{\chi p}$ analysing M82 and NGC 253 data. The SBG bounds on light dark matter particle pose strict bounds on $\sigma_{\chi p}$ at level of $10^{-31} - 10^{-34}$ cm^2 depending on the source.

References

[1] E. Peretti, P. Blasi, F. Aharonian and G. Morlino, Mon. Not. Roy. Astron. Soc. **487** (2019) no.1, 168-180 doi:10.1093/mnras/stz1161 [arXiv:1812.01996 [astro-ph.HE]].

[2] E. Peretti, P. Blasi, F. Aharonian, G. Morlino and P. Cristofari, Mon. Not. Roy. Astron. Soc. **493** (2020) no.4, 5880-5891 doi:10.1093/mnras/staa698 [arXiv:1911.06163 [astro-ph.HE]].

[3] A. Ambrosone, M. Chianese, D. F. G. Fiorillo, A. Marinelli, G. Miele and O. Pisanti, Mon. Not. Roy. Astron. Soc. **503** (2021) no.3, 4032-4049 doi:10.1093/mnras/stab659 [arXiv:2011.02483 [astro-ph.HE]].

[4] A. Ambrosone, M. Chianese, D. F. G. Fiorillo, A. Marinelli and G. Miele, Astrophys. J. Lett. **919** (2021) no.2, L32 doi:10.3847/2041-8213/ac25ff [arXiv:2106.13248 [astro-ph.HE]].

[5] A. Ambrosone, M. Chianese, D. F. G. Fiorillo, A. Marinelli and G. Miele, Mon. Not. Roy. Astron. Soc. **515** (2022) no.4, 5389-5399 doi:10.1093/mnras/stac2133 [arXiv:2203.03642 [astro-ph.HE]].

[6] A. Ambrosone, M. Chianese, D. F. G. Fiorillo, A. Marinelli and G. Miele, "Starburst Nuclei as Light

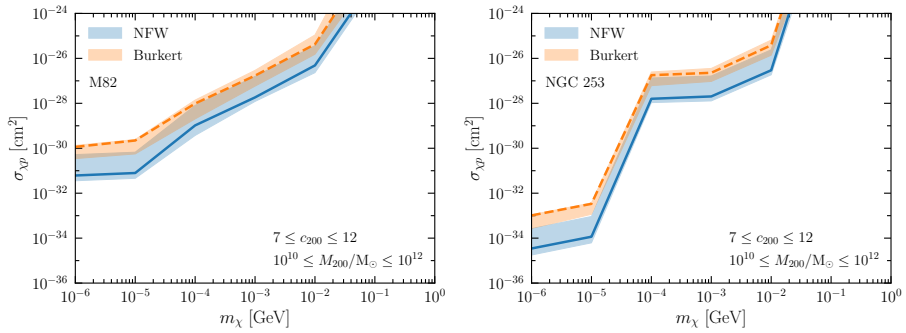

Figure 5. Left Panel $\sigma_{\chi p}$ constrains as a function of m_χ for M82. The blue band corresponds to the NFW profile, while the orange one corresponds to the Burkert one. **Right Panel** The corresponding constraints for NGC 253. Image taken from the supplementary material of Ref. [6].

Dark Matter Laboratories," [arXiv:2210.05685 [astro-ph.HE]].

[7] M. Ajello, M. Di Mauro, V. S. Paliya and S. Garrappa, Astrophys. J. **894** (2020) no.2, 88 doi:10.3847/1538-4357/ab86a6 [arXiv:2003.05493 [astro-ph.GA]].

[8] T. A. Thompson, E. Quataert, E. Waxman, N. Murray and C. L. Martin, Astrophys. J. **645** (2006), 186-198 doi:10.1086/504035 [arXiv:astro-ph/0601626 [astro-ph]].

[9] 2009Natur.462..770V VERITAS Collaboration and 92 colleagues 2009. A connection between star formation activity and cosmic rays in the starburst galaxy M82. Nature 462, 770–772. doi:10.1038/nature08557

[10] H. Abdalla *et al.* [H.E.S.S.], Astron. Astrophys. **617** (2018), A73 doi:10.1051/0004-6361/201833202 [arXiv:1806.03866 [astro-ph.HE]].

[11] P. Abreu *et al.* [Pierre Auger], Astrophys. J. **935**, no.2, 170 (2022) doi:10.3847/1538-4357/ac7d4e [arXiv:2206.13492 [astro-ph.HE]].

[12] A. Abdul Halim *et al.* [Pierre Auger], 'Constraining the sources of ultra-high-energy cosmic rays across and above the ankle with the spectrum and composition data measured at the Pierre Auger Observatory," [arXiv:2211.02857 [astro-ph.HE]].

[13] M. R. Krumholz, R. M. Crocker, S. Xu, A. Lazarian, M. T. Rosevear and J. Bedwell-Wilson, Mon. Not. Roy. Astron. Soc. **493**, no.2, 2817-2833 (2020) doi:10.1093/mnras/staa493 [arXiv:1911.09774 [astro-ph.HE]].

[14] M. A. Roth, M. R. Krumholz, R. M. Crocker and S. Celli, Nature **597**, no.7876, 341-344 (2021) doi:10.1038/s41586-021-03802-x [arXiv:2109.07598 [astro-ph.HE]].

[15] M. A. Roth, M. R. Krumholz, R. M. Crocker and T. A. Thompson, "CONGRuENTS (COsmic-ray, Neutrino, Gamma-ray and Radio Non-Thermal Spectra). I. A predictive model for galactic non-thermal emission," [arXiv:2212.09428 [astro-ph.HE]].

[16] P. Kornecki, E. Peretti, S. del Palacio, P. Benaglia and L. J. Pellizza, Astron. Astrophys. **657**, A49 (2022) doi:10.1051/0004-6361/202141295 [arXiv:2107.00823 [astro-ph.HE]].

[17] P. Kornecki, L. J. Pellizza, S. del Palacio, A. L. Müller, J. F. Albacete-Colombo and G. E. Romero, Astron. Astrophys. **641**, A147 (2020) doi:10.1051/0004-6361/202038428 [arXiv:2007.07430 [astro-ph.HE]].

[18] A. Condorelli, D. Boncioli, E. Peretti and S. Petrera, [arXiv:2209.08593 [astro-ph.HE]].

[19] E. Peretti, G. Morlino, P. Blasi and P. Cristofari, Mon. Not. Roy. Astron. Soc. **511**, no.1, 1336-1348 (2022) doi:10.1093/mnras/stac084 [arXiv:2104.10978 [astro-ph.HE]].

[20] S. R. Kelner, F. A. Aharonian and V. V. Bugayov, Phys. Rev. D **74**, 034018 (2006) [erratum: Phys. Rev. D **79**, 039901 (2009)] doi:10.1103/PhysRevD.74.034018 [arXiv:astro-ph/0606058 [astro-ph]].

[21] M. Hayashida, Ł. Stawarz, C. C. Cheung, K. Bechtol, G. M. Madejski, M. Ajello, F. Massaro, I. V. Moskalenko, A. Strong and L. Tibaldo, Astrophys. J. **779** (2013), 131 doi:10.1088/0004-637X/779/2/131 [arXiv:1310.1913 [astro-ph.HE]].

[22] B. C. Lacki and R. Beck, Mon. Not. Roy. Astron. Soc. **430**, 3171 (2013) doi:10.1093/mnras/stt122 [arXiv:1301.5391 [astro-ph.CO]].

[23] M. G. Aartsen *et al.* [IceCube], Phys. Rev. Lett. **124**, no.5, 051103 (2020) doi:10.1103/PhysRevLett.124.051103 [arXiv:1910.08488 [astro-ph.HE]].

[24] S. Aiello *et al.* [KM3NeT], Astropart. Phys. **111**, 100-110 (2019) doi:10.1016/j.astropartphys.2019.04.002 [arXiv:1810.08499 [astro-ph.HE]].

[25] S. Adrian-Martinez *et al.* [KM3Net], J. Phys. G **43**, no.8, 084001 (2016) doi:10.1088/0954-3899/43/8/084001 [arXiv:1601.07459 [astro-ph.IM]].

[26] B. S. Acharya *et al.* [CTA Consortium], WSP, 2018, ISBN 978-981-327-008-4 doi:10.1142/10986 [arXiv:1709.07997 [astro-ph.IM]].

[27] F. G. Saturni, C. H. E. .Arcaro, B. .Balmaverde, J. B. González, A. Caccianiga, M. Capalbi, A. .Lamastra, S. Lombardi, F. Lucarelli and R. Alves Batista, *et al.* JHEAp **35**, 91-111 (2022) doi:10.1016/j.jheap.2022.06.004 [arXiv:2208.03176

[astro-ph.HE]].

[28] S. Scuderi, A. Giuliani, G. Pareschi, G. Tosti, O. Catalano, E. Amato, A. L. A., J. Becerra Gonzàles, G. Bellassai and C. Bigongiari, *et al.* JHEAp **35**, 52-68 (2022) doi:10.1016/j.jheap.2022.05.001 [arXiv:2208.04571 [astro-ph.IM]].

[29] A. Albert, R. Alfaro, H. Ashkar, C. Alvarez, J. Alvarez, J. C. Arteaga-Velázquez, H. A. Ayala Solares, R. Arceo, J. A. Bellido and S. BenZvi, *et al.* [arXiv:1902.08429 [astro-ph.HE]].

[30] Y. Ema, F. Sala and R. Sato, SciPost Phys. **10**, no.3, 072 (2021) doi:10.21468/SciPostPhys.10.3.072 [arXiv:2011.01939 [hep-ph]].

[31] G. Guo, Y. L. S. Tsai, M. R. Wu and Q. Yuan, Phys. Rev. D **102**, no.10, 103004 (2020) doi:10.1103/PhysRevD.102.103004 [arXiv:2008.12137 [astro-ph.HE]].

[32] R. H. Cyburt, B. D. Fields, V. Pavlidou and B. D. Wandelt, Phys. Rev. D **65**, 123503 (2002) doi:10.1103/PhysRevD.65.123503 [arXiv:astro-ph/0203240 [astro-ph]].

[33] D. Hooper and S. D. McDermott, Phys. Rev. D **97**, no.11, 115006 (2018) doi:10.1103/PhysRevD.97.115006 [arXiv:1802.03025 [hep-ph]].

[34] F. Iocco, M. Pato and G. Bertone, Nature Phys. **11**, 245-248 (2015) doi:10.1038/nphys3237 [arXiv:1502.03821 [astro-ph.GA]].

[35] G. Bertone and D. Hooper, Rev. Mod. Phys. **90**, no.4, 045002 (2018) doi:10.1103/RevModPhys.90.045002 [arXiv:1605.04909 [astro-ph.CO]].

[36] P. Salucci, "The distribution of dark matter in galaxies," Astron. Astrophys. Rev. **27**, no.1, 2 (2019) doi:10.1007/s00159-018-0113-1 [arXiv:1811.08843 [astro-ph.GA]].

[37] M. Werhahn, C. Pfrommer, P. Girichidis and G. Winner, Mon. Not. Roy. Astron. Soc. **505**, no.3, 3295-3313 (2021) doi:10.1093/mnras/stab1325 [arXiv:2105.11463 [astro-ph.HE]].

[38] M. Werhahn, C. Pfrommer, P. Girichidis, E. Puchwein and R. Pakmor, Mon. Not. Roy. Astron. Soc. **505**, no.3, 3273-3294 (2021) doi:10.1093/mnras/stab1324 [arXiv:2105.10509 [astro-ph.HE]].

[39] M. Werhahn, C. Pfrommer and P. Girichidis, Mon. Not. Roy. Astron. Soc. **508**, no.3, 4072-4095 (2021) doi:10.1093/mnras/stab2535 [arXiv:2105.12134 [astro-ph.GA]].

[40] C. Pfrommer, M. Werhahn, R. Pakmor, P. Girichidis and C. M. Simpson, Mon. Not. Roy. Astron. Soc. **515**, no.3, 4229-4264 (2022) doi:10.1093/mnras/stac1808 [arXiv:2105.12132 [astro-ph.GA]].

[41] M. Werhahn, P. Girichidis, C. Pfrommer and J. Whittingham, [arXiv:2301.04163 [astro-ph.HE]].

[42] M. Benito, N. Bernal, N. Bozorgnia, F. Calore and F. Iocco, JCAP **02**, 007 (2017) [erratum: JCAP **06**, E01 (2018)] doi:10.1088/1475-7516/2017/02/007 [arXiv:1612.02010 [hep-ph]].

[43] J. F. Navarro, C. S. Frenk and S. D. M. White, Astrophys. J. **462**, 563-575 (1996) doi:10.1086/177173 [arXiv:astro-ph/9508025 [astro-ph]].

[44] A. Burkert, Astrophys. J. Lett. **447**, L25 (1995) doi:10.1086/309560 [arXiv:astro-ph/9504041 [astro-ph]].

[45] A. Franceschini and G. Rodighiero, Astron. Astrophys. **603**, A34 (2017) doi:10.1051/0004-6361/201629684 [arXiv:1705.10256 [astro-ph.HE]].